Efficient Methods of Measuring Shielding Effectiveness of Electrically Large Enclosures Using Nested Reverberation Chambers with Only Two Antennas

Zhihao Tian, *Student Member, IEEE*, Yi Huang, *Senior Member, IEEE*, and Qian Xu

***Abstract*—Measuring the shielding effectiveness (SE) of physically small but electrically large enclosures is an important concern in electronics industry. In recent years, reverberation chambers (RCs) are becoming prevalent in determining the SE of such enclosures. Conventionally, frequency-domain (FD) measurement is adopted. It requires three antennas (one transmitting antenna and one receiving antenna in the large RC and one receiving antenna in the nested small enclosure). Furthermore, to obtain good accuracy, the knowledge of the efficiency of the two receiving antennas is also required. To promote the industrial application of RCs for SE measurement, simplified methods are desired. In this paper, simplified measurement methods are proposed and studied both in the FD and the time domain (TD). Only two antennas are required in the proposed methods. Thus the measurement setup is greatly simplified. It is found that in the TD, a fast and accurate measurement method can be realized with the simplified measurement setup. Moreover, the measurement simplification can go a step further by replacing the RC with an electrically large metallic enclosure in the TD. The measurement results demonstrate that the TD approach outperforms the FD approach in many ways. The proposed methods have the merits of high efficiency, good accuracy, and simple measurement setups. They are very suitable for SE measurement of electrically large enclosures.**

***Index Terms*— Electromagnetic interference, electrically large enclosure, frequency domain, nested reverberation chamber, shielding effectiveness, source stirring, time domain.**

I. Introduction

ELECTROMAGNETIC shielding has become a significant issue due to the proliferation of electronic devices in the world. Shielding enclosures are used to either protect or control immunity and/or emission of electronic devices for many applications. The shielding effectiveness (SE) is an important figure of merit to characterize the electromagnetic isolation performance of the enclosures.

Generally, an IEEE standard can be followed for measuring the SE of electromagnetic shielding enclosures [1] in an anechoic chamber. The idea is to illuminate the equipment under test (EUT) with a plane wave, and consequently only several incidence directions and polarizations can be tested in practice. However, in real-life, equipment is seldom exposed to a single plane wave; a more realistic scenario would be waves coming from different directions. Recently, the reverberation chamber (RC) technique is becoming prevalent for the SE measurement [2]-[9]. The use of RCs for determining the SE has the advantage over other techniques in that the RC offers a more realistic environment. That is, in an RC, the fields are incident on the EUT with various polarizations and angles of incidence [10].

Conventionally, to measure the SE of an electrically large enclosure in an RC, we need to set a transmitting antenna (T_x) along with a receiving antenna in the large RC (R_{xo}) and a receiving antenna inside the nested small enclosure (R_{xi}). By comparing the power transfer functions (PTFs) between $T_x - R_{xo}$ and between $T_x - R_{xi}$ in the frequency domain (FD), the SE of the small enclosure can be extracted. However, this approach requires three antennas and the knowledge of the efficiency of the two receiving antennas, which could be problematic sometimes in practice. An optional time-domain (TD) method proposed in [5] is to use the decay time of the enclosure to extract SE. But it needs to cover and uncover the aperture of the enclosure which may not be applicable for some equipment with complex structures. And also, when the EUT is well shielded, the measurement uncertainty increases very quickly.

In this paper, we propose four improved measurement methods for SE measurement of electrically large enclosures using a nested RC. Both the FD and the TD methods are studied. The proposed methods require only two antennas and provide efficient measurement of SE without losing the accuracy.

This paper consists of five sections. Section II derives the equations of the proposed methods for the measurement of SE

Manuscript received ***. (*Corresponding author: Yi Huang.*)

Zhihao Tian is with the Department of Electrical Engineering and Electronics, University of Liverpool, Liverpool L69 3GJ, U.K., and also with the College of Optoelectronic Science and Engineering, National University of Defense Technology, Changsha 410073, China (e-mail: zhihao.tian@liv.ac.uk).

Yi Huang is with the Department of Electrical Engineering and Electronics, University of Liverpool, Liverpool L69 3GJ, U.K. (e-mail: yi.huang@liv.ac.uk).

Qian Xu is with the College of Electronic and Information Engineering, Nanjing University of Aeronautics and Astronautics, Nanjing 210000, People's Republic of China. (e-mail: emxu@foxmail.com).

in the FD and in the TD. Section III details the measurement procedures. And the measured SEs of the EUT using different methods are compared in this section. The continued convergence behaviour analysis of the proposed approaches is given in Section IV. Finally, the discussion and conclusions are given in Section V.

II. Theoretical Analysis

It has been shown that for a well-stirred electrically large enclosure, the SE of the enclosure is defined as follows:

$$\mathrm{SE} = -10\log_{10}\frac{\langle P_{in}\rangle}{\langle P_{out}\rangle} \tag{1}$$

or

$$\mathrm{SE} = -10\log_{10}\frac{\langle S_{in}\rangle}{\langle S_{out}\rangle} \tag{2}$$

where P_{in} and P_{out} are the power levels inside and outside the enclosure, S_{in} and S_{out} are the power density levels inside and outside the enclosure, respectively. $\langle\cdot\rangle$ denotes an ensemble average for all stirring sequences.

A. FD Method

In the FD, the existing measurement method of determining the SE is to compare the PTFs between $T_x - R_{xo}$ and between $T_x - R_{xi}$. The PTF can be obtained from the *S*-parameter as [11]:

$$\frac{\langle P_r\rangle}{P_t} = \langle|S_{21}|^2\rangle \tag{3}$$

where $\langle P_r\rangle$ is the average received power either in the RC or in the EUT, P_t is the transmitting power in the RC. Again, $\langle\cdot\rangle$ represents an ensemble average for all stirring sequences. This *S*-parameter can be measured using a vector network analyser (VNA). Actually, $\langle|S_{21}|^2\rangle$ is an uncalibrated PTF. The ohmic loss of antennas, the antennas mismatch, and also, both the stirred and unstirred power in the chamber are included [3], [12], [13]. The net PTF T can be obtained by removing the ohmic loss and mismatch of antennas as [11], [12]:

$$T = \frac{\langle|S_{21,s}|^2\rangle}{(1-|\langle S_{11}\rangle|^2)(1-|\langle S_{22}\rangle|^2)\eta_1^{rad}\eta_2^{rad}} \tag{4}$$

where $S_{21,s}$ represents the stirred power contribution of S_{21}. It is obtained by correcting the mismatch effect [3], [12]:

$$S_{*,s} = S_* - \langle S_*\rangle \tag{5}$$

$\langle\cdot\rangle$ signifies the ensemble average using any stirring method (mode stirring [10], frequency stirring [14], source stirring [15], *etc.*), η_1^{rad} and η_2^{rad} are the efficiency of the transmitting and the receiving antennas, respectively.

In the following analysis, the transmitting antenna in the RC is denoted by antenna 1, the receiving antenna in the RC is denoted by antenna 2 and the receiving antenna in the EUT is denoted by antenna 3, as can be seen from Fig. 1 (a). Then, the net PTF in the RC (T_o) can be extracted as:

$$T_o = \frac{\langle|S_{21,s}|^2\rangle}{(1-|\langle S_{11}\rangle|^2)(1-|\langle S_{22}\rangle|^2)\eta_1^{rad}\eta_2^{rad}} \tag{6}$$

where η_1^{rad} and η_2^{rad} are the efficiency of antenna 1 and antenna 2, respectively. The net PTF between the RC and the EUT (T_i) can be given as:

$$T_i = \frac{\langle|S_{31,s}|^2\rangle}{(1-|\langle S_{11}\rangle|^2)(1-|\langle S_{33}\rangle|^2)\eta_1^{rad}\eta_3^{rad}} \tag{7}$$

where η_3^{rad} are the efficiency of antenna 3.

Substituting (3), (6) and (7) into (1), the SE can be determined from ratio of the net PTFs T_i and T_o:

$$\begin{aligned}\mathrm{SE} &= -10\log_{10}\left(\frac{T_i}{T_o}\right)\\ &= -10\log_{10}\left(\frac{\langle|S_{31,s}|^2\rangle}{\langle|S_{21,s}|^2\rangle}\cdot\frac{1-|\langle S_{22}\rangle|^2}{1-|\langle S_{33}\rangle|^2}\cdot\frac{\eta_2^{rad}}{\eta_3^{rad}}\right)\end{aligned} \tag{8}$$

As can be seen from (8), three antennas are needed in the measurement. Typically, the net PTFs are measured with two high-efficiency antennas using (6) and (7) with the knowledge of their efficiency (η_2^{rad}, η_3^{rad}). And also, for the measurement using a two-port VNA, two measurements are required (connecting receiving port to antenna 2 and antenna 3, respectively), which is really time consuming.

If an RC is ideally performing, we have the enhanced backscatter constant [11], [16], [17]

$$e_b = \sqrt{\langle|S_{11,s}|^2\rangle\langle|S_{22,s}|^2\rangle}\Big/\langle|S_{21,s}|^2\rangle = 2 \tag{9}$$

Assuming antenna 1 and antenna 2 are identical, we can obtain $\langle|S_{11,s}|^2\rangle = \langle|S_{22,s}|^2\rangle = 2\langle|S_{21,s}|^2\rangle$. Now, equation (6) can be converted to the form [11]:

$$T_o = \frac{\langle|S_{11,s}|^2\rangle}{2(1-|\langle S_{11}\rangle|^2)^2(\eta_1^{rad})^2} \tag{10}$$

Substituting (10) into (8), the SE can be rewritten as:

$$\mathrm{SE} = -10\log_{10}\left(2\cdot\frac{\langle|S_{31,s}|^2\rangle}{\langle|S_{11,s}|^2\rangle}\cdot\frac{1-|\langle S_{11}\rangle|^2}{1-|\langle S_{33}\rangle|^2}\cdot\frac{\eta_1^{rad}}{\eta_3^{rad}}\right) \tag{11}$$

Thus, only two antennas are needed (one transmitting antenna in the RC and one receiving antenna in the EUT) and the measurement can be completed once, which will greatly

simplify the measurement. The precondition for this method is $e_b = 2$. The impact of e_b to the validity of this method will be discussed in Section IV. If the transmitting antenna in the RC and the receiving antenna in the EUT are identical, (11) can be further simplified as:

$$\mathrm{SE} = -10\log_{10}\left(2 \cdot \frac{\langle |S_{31,s}|^2 \rangle}{\langle |S_{11,s}|^2 \rangle}\right) \tag{12}$$

It is interesting to note that the efficiency is eliminated in (12) and we do not have to get the knowledge of the efficiency of any antenna used in the measurement – the condition is both antennas are identical.

B. TD Method

In the TD, the reverberant diffuse fields in each cavity, denoted by subscript $i = 1, 2$, are analyzed based on the time-dependent full exchange of radiated electromagnetic power between coupled spaces [8], [18]-[20]. The spatially averaged power density is modeled from conservation of energy consideration when the excitation source is in cavity 1:

$$V_1\langle \dot{S_1}(t)\rangle = -(\Lambda_1 + \Lambda_t)\langle S_1(t)\rangle + \Lambda_t\langle S_2(t)\rangle + \delta(t) \tag{13}$$

$$V_2\langle \dot{S_2}(t)\rangle = \Lambda_t\langle S_1(t)\rangle - (\Lambda_2 + \Lambda_t)\langle S_2(t)\rangle \tag{14}$$

where $\langle S_i \rangle$ is the averaged power density in cavity *i*, $\langle \dot{S_i}(t)\rangle$ signifies the time rate of change of the averaged power density of cavity *i*. V_i is the volume of cavity *i* and $\delta(t)$ is an impulse of electromagnetic power fed to the cavity at time $t = 0$. Λ_i and Λ_t are the energy loss rate coefficients for cavity *i* and for coupling between the two cavities, respectively [20].

The analytical solutions to (13) and (14) are provided [21], [22]

$$\langle S_1(t)\rangle = \frac{U_0}{\alpha - \beta}\left[\frac{\alpha e^{\alpha t} - \beta e^{\beta t}}{V_1} + \frac{(\Lambda_1 + \Lambda_2)\left(e^{\alpha t} - e^{\beta t}\right)}{V_1 V_2}\right] \tag{15}$$

$$\langle S_2(t)\rangle = \frac{U_0\Lambda_t}{V_1 V_2} \cdot \frac{e^{\alpha t} - e^{\beta t}}{\alpha - \beta} \tag{16}$$

where the coefficients α and β are defined according to the relationships shown in (17) and (18):

$$B = \frac{\Lambda_2 + \Lambda_t}{V_2} + \frac{\Lambda_1 + \Lambda_t}{V_1}, \quad C = \frac{\Lambda_1\Lambda_2 + \Lambda_1\Lambda_t + \Lambda_2\Lambda_t}{V_1 V_2} \tag{17}$$

$$\alpha = \frac{-B + \sqrt{B^2 - 4C}}{2}, \quad \beta = \frac{-B - \sqrt{B^2 - 4C}}{2} \tag{18}$$

and U_0 is the total power injected into cavity 1 by the impulse excitation at time $t = 0$.

(15) and (16) can be rewritten as:

$$\langle U_1(t)\rangle = \frac{U_0}{\alpha - \beta}\left[(\alpha + \frac{\Lambda_1 + \Lambda_2}{V_2})e^{\alpha t} - (\beta + \frac{\Lambda_1 + \Lambda_2}{V_2})e^{\beta t}\right] \tag{19}$$

$$\langle U_2(t)\rangle = \frac{U_0\Lambda_t}{V_1} \cdot \frac{e^{\alpha t} - e^{\beta t}}{\alpha - \beta} \tag{20}$$

where $\langle U_1(t)\rangle$ and $\langle U_2(t)\rangle$ are the averaged total power in cavity 1 and cavity 2, respectively. (19) and (20) describe the dynamics of power level inside the RC (cavity 1) and the EUT (cavity 2) when a short pulse is injected into the RC. As we can see, the TD response of the RC and the EUT is of double-exponential behaviour [23]. The transient response of $\langle U_1(t)\rangle$ and $\langle U_2(t)\rangle$ can be obtained by fitting the power delay profiles (PDP) of the RC and the EUT, respectively. This fitting process can be realized through a least-square-fit optimization routine that minimizes the sum of the squares of the error between overlaid modeled and measured curves. The SE of the EUT can then be obtained by the difference of the fitted PDP (in dB format) of the RC (PDP_{RC}) and that of the EUT (PDP_{EUT}) [20]:

$$\mathrm{SE(dB)} = PDP_{RC}(\mathrm{dB}) - PDP_{EUT}(\mathrm{dB}) \tag{21}$$

The PDP_{RC} and PDP_{EUT} are obtained from S_{21} data and S_{31} data, respectively. For an ideally stirred RC, it has been proved that in the TD [16]

$$e_b = \frac{\sqrt{PDP_{RC}^{S11} \cdot PDP_{RC}^{S22}}}{PDP_{RC}^{S21}} = 2 \tag{22}$$

where PDP_{RC}^{S11}, PDP_{RC}^{S22} and PDP_{RC}^{S21} (in linear format) are the PDPs (excluding the early-time part) of the RC from the S_{11}, S_{22} and S_{21} data, respectively. Likewise, assuming antenna 1 and antenna 2 are identical, (22) then becomes

$$PDP_{RC}^{S21} = \frac{1}{2} \cdot PDP_{RC}^{S11} \tag{23}$$

Or in dB format,

$$PDP_{RC}^{S21}(\mathrm{dB}) = PDP_{RC}^{S11}(\mathrm{dB}) - 3\mathrm{dB} \tag{24}$$

And (21) can be rewritten as

$$\mathrm{SE(dB)} = PDP_{RC}^{S11}(\mathrm{dB}) - 3\mathrm{dB} - PDP_{EUT}(\mathrm{dB}) \tag{25}$$

Thus, antenna 2 is eliminated in (25) and the two-antenna method in the TD is mathematically derived.

III. Measurement and Results

Measurements were conducted from 2.8 to 4.2 GHz in our RC to verify the proposed methods. The size of the RC is 3.6 m × 4.0 m × 5.8 m. Two mode-stir paddles are installed in the RC: the vertical one is mounted in a corner and the horizontal one is mounted close to the ceiling. In our measurement, three antennas were used: two double-ridged waveguide horn

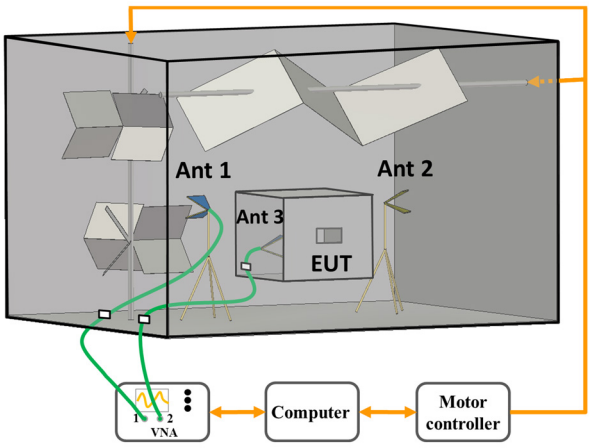

(a)

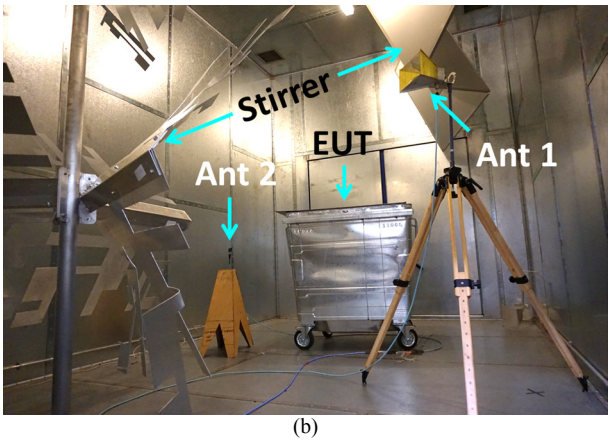

(b)

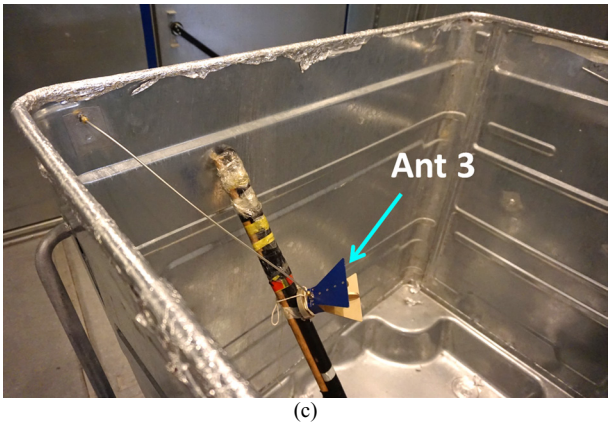

(c)

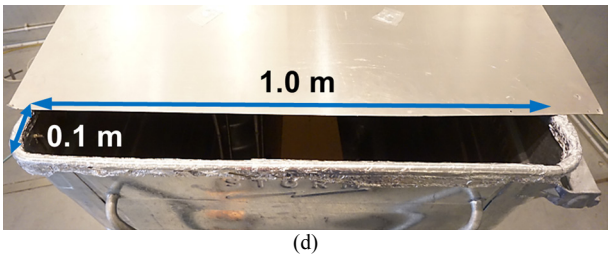

(d)

Fig. 1. SE measurement setup in the RC: (a) measurement system, (b) measurement setup in the experiment, (c) antenna 3 (SATIMO horn antenna) in the EUT, (d) the aperture of the EUT.

antennas were used as antenna 1 (Rohde & Schwarz HF 906) and antenna 3 (SATIMO SH 2000), respectively, one planar monopole antenna was used as antenna 2. We connected antenna 1 to VNA port 1 and connected antenna 2 (or antenna 3) to VNA port 2. The step-by-step rotation of the two stirrers was synchronized. 360 positions were obtained (1 degree per step). For each mode stirring position, the VNA swept over the full frequency span and recorded the *S*-parameters. A metallic enclosure with an open-air aperture is employed as the EUT. The EUT has a size of 1.0 m × 1.0 m × 1.1 m (about 10 λ × 10 λ × 11 λ at 3.0 GHz). The size of the aperture is about 1.0 m × 0.1 m. According to Weyl's formula [3], [24], the mode number is around 9,185 inside the EUT at 3.0 GHz, which is large enough for the RC to perform well. The whole measurement system is depicted in Fig. 1 (a). Fig. 1 (b) and Fig. 1 (c) illustrate the measurement setup and the detail of the aperture is shown in Fig.1 (d).

The measurement is performed according to the following procedure.

Step 1: Do standard calibration process of the VNA including the cables.
Step 2: Place antenna 1 and antenna 2 inside the RC and place antenna 3 inside the EUT. Place all the antenna supports along with the antennas inside the RC to keep the chamber loss constant.
Step 3: Connect antenna 1 to port 1 of the VNA and antenna 2 to port 2 of the VNA, load antenna 3 with a 50 Ω termination and collect the full *S*-parameters for each stirring position.
Step 4: Repeat *Step 3* with antenna 3 connected to port 2 of the VNA and antenna 2 loaded with a 50 Ω termination.

In practise, it may not have a chance to introduce mode stirring or source stirring in the EUT, thus only frequency stirring is used here. In the measurement, 10,001 points were sampled in the frequency span of 2.8 to 4.2 GHz. The conventional 3-antenna method ($SE_{FD,3}$), the 2-antenna method in the FD ($SE_{FD,2}$) and the 2-antenna method in the TD ($SE_{TD,2}$) were adopted respectively to calculate the SE of the EUT. To make the abbreviation clear, "2" or "3" is assigned to the second subscript to signify that two or three antennas were used in the measurement. In the FD, the enhanced backscatter constant (e_b) is calculated and plotted in Fig. 2. As can be seen, it is close to 2. This means the RC was well performing and the experiment equipment was reasonably set up [11], [16]. The PTFs of the RC measured using antenna 1 ($T_{o,1}$) and using antenna 1 and antenna 2 ($T_{o,2}$) are shown in Fig. 3. The PTF from the RC to the EUT ($T_{i,2}$) measured using antenna 1 and antenna 3 is plotted in Fig. 3 as well. Again, to make the abbreviation clear, "*o*" or "*i*" is assigned to the first subscript to signify that the measurement was done when the receiving antenna was outside or inside the EUT. "1" or "2" in the second subscript means one or two antennas were required in the measurement. As can be seen, $T_{i,2}$ is smaller than $T_{o,1}$ and $T_{o,2}$ because of the shielding of the EUT. $T_{o,1}$ agrees well with $T_{o,2}$, which manifests that the two-antenna method for SE measurement in the FD is effective. Since the data was measured in the FD, we attain the TD method by applying the inverse Fourier transform (IFT) on the measured data. In the

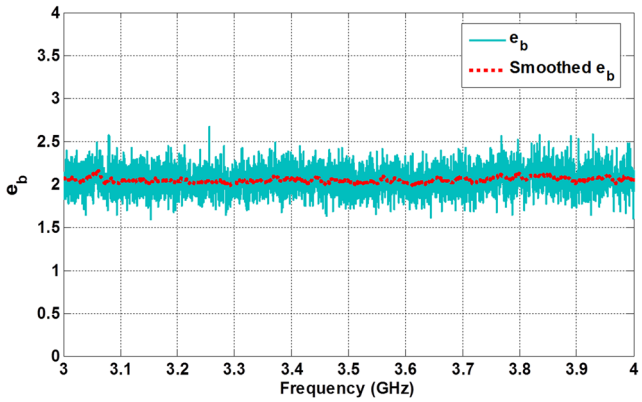

Fig. 2. The measured e_b in the RC.

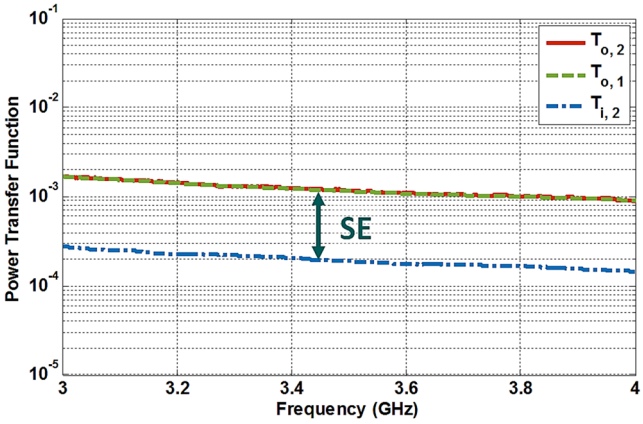

Fig. 3. The measured PTFs in the RC and between the RC and the EUT.

TD, we used a 10-order band-pass elliptic filter to filter S_{11} and S_{31} with a 200-MHz bandwidth [11], as can be seen from Fig. 4. Since the transient responses of the power in the RC and in the EUT are of double exponential behaviour, the least-square-fit optimization is applied to the PDPs and the modeled decay behaviour can be obtained, as shown in Fig. 5 (a). The dynamics of power transfer between the RC and the EUT are of particular interest. As can be seen from Fig. 5 (b), early-time behaviour is observed because of the unstirred reflections from the antenna itself and from the walls of the RC [20]. For $P_2(t)$, at the first 200 ns, it rises slowly and the energy in the RC must leak into the EUT gradually through the leakage aperture described by Λ_t. After the EUT is fully filled, $P_2(t)$ ultimately decreases along with $P_1(t)$. It can be noticed, at the first 20 ns, no rise appears for $P_2(t)$ because the power emitting from the T_x antenna takes certain time to reach the R_x antenna. The 20 ns correspond to about 6 meters for electromagnetic wave travelling in free space, which agrees well with the distance between antenna 1 and antenna 3 in the experiment. The difference between $P_1(t)$ and $P_2(t)$ at the late time gives us the information of SE of the EUT. It is worth noting that, to avoid the influence of the early-time behaviour, only part of the PDPs (the late-time part) should be used to evaluate the SE. The results are illustrated in Fig. 6. 200-MHz frequency stirring is used in the FD. The efficiency of antenna 1, antenna 2 and antenna 3 in 3.0-4.0 GHz are 95%, 80% and 82%, respectively. When conducting the measurement using the two-identical-antenna method, antenna 1 was replaced with another SATIMO SH 2000 horn antenna. It can be seen clearly

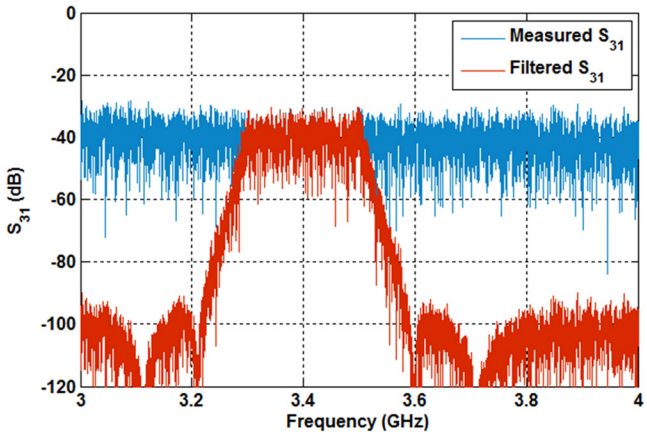

Fig. 4. Measured S_{31} and filtered S_{31}.

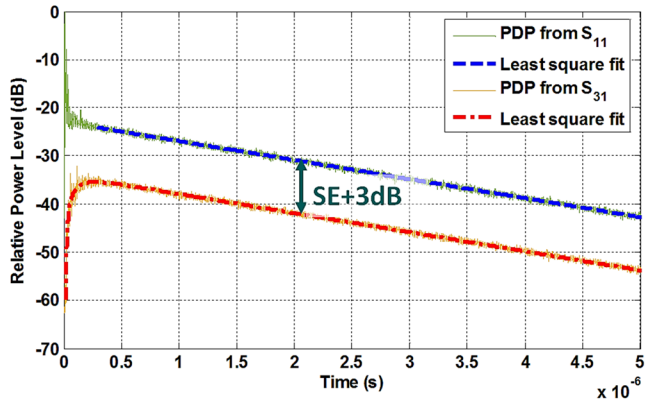

(a)

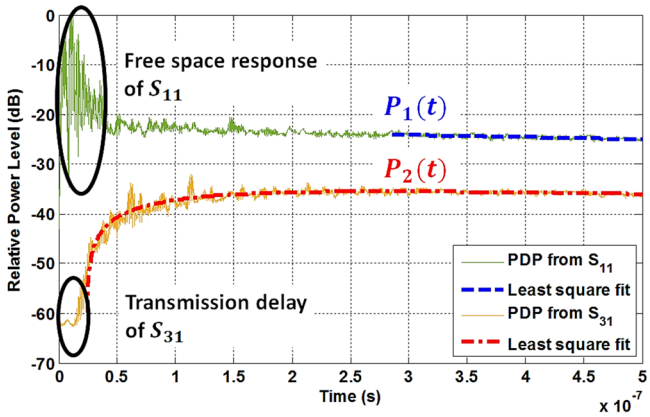

(b)

Fig. 5. Transient responses of the PDPs in the RC and in the EUT for the impulse excitation injected into the RC: (a) PDPs from S_{11} and from S_{31}, respectively, (b) early-time responses of PDPs.

from Fig. 6 that the measured SEs using the four methods agree well and the maximum difference is within 0.5 dB.

IV. Convergence Behaviour

The convergence behaviour of the proposed two-antenna methods in the FD and in the TD is studied as well.

As indicated in (9) and (10), the two-antenna method in the FD requires $e_b = 2$. A basic question is "what is the impact of of e_b to the validity of the FD measurement method?" That is, if e_b deviates from 2, what kind of results should be expected?

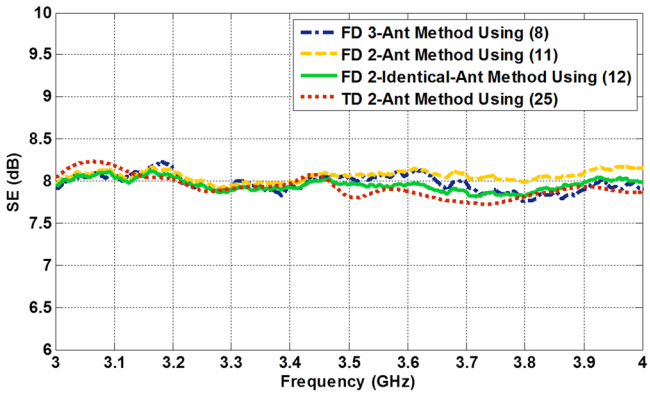

Fig. 6. The SEs of the EUT measured with different methods.

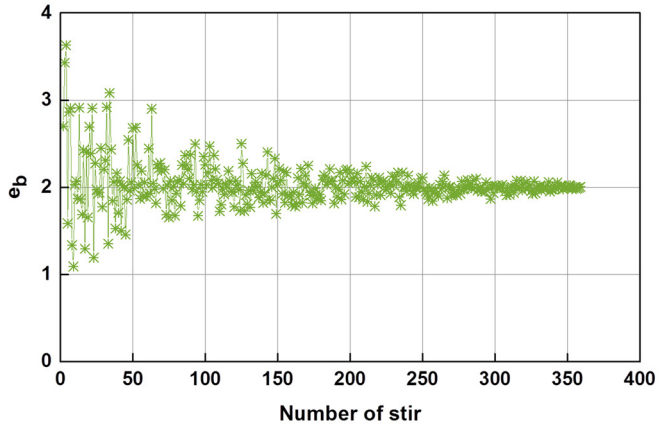

(a)

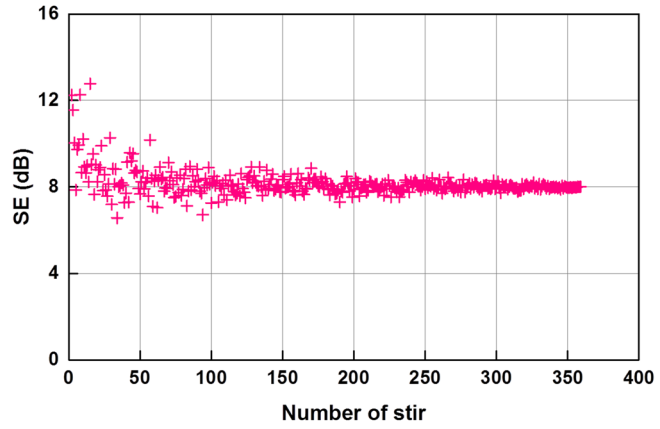

(b)

Fig. 7 The convergence properties of (a) e_b, and (b) $SE_{FD,2}$ at 3.5 GHz.

In fact, intuition and experience say that if e_b deviates from 2 a lot, the measured SE should be unreliable because the field in the RC is not well stirred, i.e., the field is not statistically uniform. To investigate this issue, we checked the variation of the measured $SE_{FD,2}$ along with e_b at 3.5 GHz where the SE is 8 dB, as shown in Fig. 7 (a) and Fig. 7(b). We can clearly see that the deviation of e_b from 2 fluctuates intensely at about the first 50 stirring positions. Consequently, the measured SE is inaccurate as expected. The maximum difference can reach about 90%. However, e_b begins to converge to 2 gradually with the stirring positions number increasing. For $SE_{FD,2}$, its

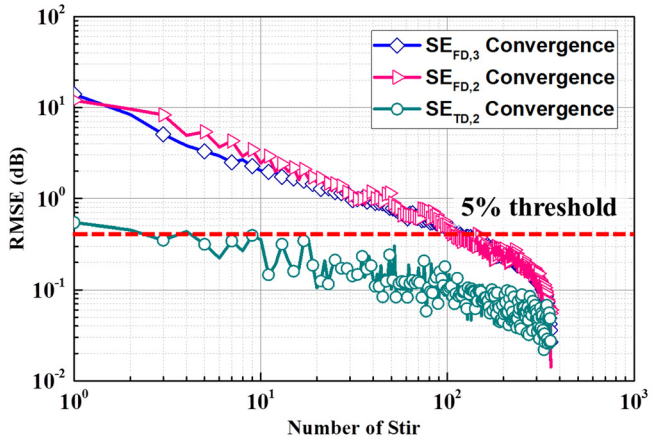

Fig. 8 The comparison of RMSEs of different methods.

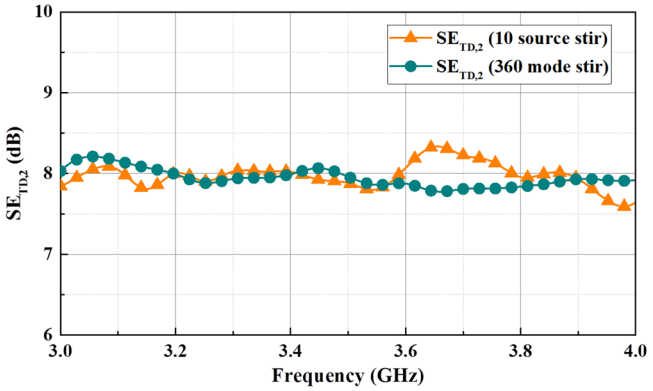

Fig. 9 The comparison of $SE_{TD,2}$ (10 source stirring positions) and $SE_{TD,2}$ (360 mode stirring positions).

convergence behaviour is coincident with e_b. The measured $SE_{FD,2}$ becomes stable (it converges to 8 dB) after about 250 stirring positions when the variation of e_b from 2 becomes very small (within 10% variation). From the above analysis, we gain the knowledge that the accuracy of the FD two-antenna method relies on $e_b = 2$. That is to say, the FD measurement is sensitive to the deviation of the chamber field from the ideally over-moded case.

The convergence behaviour of the proposed two-antenna methods in the TD is studied by comparing it with the convergence behaviour in the FD. We begin by evaluating the root-mean-square-error (RMSE) of the measured SE from 3.0-4.0 GHz with different numbers of stirring positions [11]. The reference we have is the SE measured with 360 stirring positions. The algorithm is expressed as:

$$\mathrm{RMSE}_i = \sqrt{\frac{\sum_{j=1}^{N}\left(\mathrm{SE}_{i,j} - \mathrm{SE}_{M,j}\right)^2}{N}} \tag{26}$$

In (26), i represents the number of stirring positions and M is the maxima of i. j signifies the frequency sampling point number and N is the maximal value of j. In our measurement, M = 360 and N = 7144. The comparison of RMSEs of different methods is depicted in Fig. 8. As can be seen, the convergence speeds of the two-antenna method and the three-antenna method in the FD are close but the TD method converges faster

TABLE I
SUMMARY OF THE EXISTING METHODS AND THE PROPOSED METHODS

Measurement method	Number of antennas required	Antenna efficiency requirement	Measurement times	Measurement time	Measurement facility
FD 3-antenna method	3	Yes	2	About 14 hrs	RC
FD 2-antenna method	2	Yes	1	About 7 hrs	RC
FD 2-identical-antenna method	2	No	1	About 7 hrs	RC
TD 2-antenna method (mode stirring)	2	No	1	About 10 mins	RC
TD 2-antenna method (source stirring)	2	No	1	About 10 mins	Electrically large cavity
TD 1-antenna method proposed in [5]	1	No	2	About 20 mins	EUT only

than the FD methods. This is because the PTF and e_b are very sensitive to deviations of the chamber field from the ideally over-moded case (i.e., how well the RC is stirred). But, the modeled PDP is not susceptible to the boundary conditions. It is mainly determined by the diffuse loss of the RC. That means the PDP is very robust. In other words, the TD measurement is far less sensitive to the non-ideal chamber field and appears to yield an average of the PDP. As a result, $\mathrm{SE}_{\mathrm{TD},\,2}$ converges faster than $\mathrm{SE}_{\mathrm{FD},\,2}$ and $\mathrm{SE}_{\mathrm{FD},\,3}$. To be more specific, in the TD, the RMSE remains less than 10% (in comparison with the averaged SE in the frequency span of interest, about 8 dB from Fig. 6.) and drops below 5% after about 10 stirring positions. However, in the FD, the RMSEs of the two-antenna method and the three-antenna method drop below 5% after about 100 stirring positions. And also, the RMSEs keep exceeding 10% for the first 40 stirring positions and then decline gradually afterwards.

From above analysis, we know that the PDP is robust and the TD method converges fast. Actually, these properties offer us a way to obtain SE with a small number of stirring positions and subsequently result in an efficient measurement method of SE. Basically, for a small number of stirring positions case, source-stir technique can be adopted, which will avoid rotating the stirrers. In practice, the measurement can be completed in an electrically large conducting cavity, i.e., no mode-stirred RC is required. By doing this, the measurement simplification can go a step further. To validate this idea, another set of measurement was performed. In this measurement, the RC stirrers were kept fixed (no mode stirring introduced). Consequently, the RC would just serve as an electrically large enclosure. In order to recover the true PDP, we rotated a turn-table platform on which the transmitting antenna was mounted (thus the source was rotated). Considering the convergence speed of $\mathrm{SE}_{\mathrm{TD},2}$, we chose 10 source stirring positions. The turn-table platform was rotated stepwise to 10 positions (36 degrees for each step). Antenna 1 (Rohde & Schwarz HF 906) was mounted on the turn-table platform and connected to VNA port 1. Antenna 2 (SATIMO SH 2000) was placed inside the EUT and connected to VNA port 2. The PDPs of the outer cavity (i.e., the RC with stirrers being fixed) and between the outer cavity and the EUT were extracted from S_{11} and S_{21}, respectively. The measured SEs are plotted in Fig. 9. We see that the SEs measured using 360 mode stirring positions and 10 source stirring positions agree well and the maximal variation is less than 10%. Also, the entire time consumed by the source-stir measurement was only approximately 10 minutes. It signifies that the SE can be measured in the TD instantly and precisely. The consumed time of this method is comparable with the one proposed in [5]. But it is more advisable for EUTs with complex structures because we do not need to cover and uncover the apertures. And therefore, it is quite general and efficient for SE measurement of electrically large enclosures. The aforementioned measurement methods are compared and summarized in Table I. Because the measurement accuracy relies on the number of independent samples in measurement sequences, a sufficient number of independent samples should be obtained at the lowest frequency of the measurement. This makes a request for the size of the outer cavity – it should be suitably large to accommodate sufficient cavity modes. When selecting the outer cavity for the measurement, its size should be carefully considered.

V. DISCUSSIONS AND CONCLUSIONS

In this paper, the two-antenna methods for the SE measurement using the nested RC in both the FD and the TD have been presented. These two-antenna methods have simplified the measurement setup and improved the measurement efficiency. It is demonstrated that the measured SEs using the proposed two-antenna methods and the conventional three-antenna method agree well. The TD method goes to convergence much faster than the FD methods. Consequently, in the TD, fast and accurate measurement can be realized by using the source-stir technique, which will result in fast SE measurement in reality. Furthermore, in the TD approach, by replacing the RC with suitable conducting cavity (electrically large) and using the source-stir technique, the hardware requirement will be greatly reduced. The aforementioned measurement methods are compared. It is found that the TD method outperforms the FD method with much higher measurement efficiency and much lower hardware requirement.

Note that the proposed methods are based on the assumption that both the RC and the EUT are well stirred, if not, the measured PTF and PDP will be of considerable errors. Hence, the measured SE will be inaccurate. Another point that should be noted is that high-efficiency antennas should be used for the TD method, i.e., the loss of the antennas used in the measurement should be negligible. Otherwise, the measured PDP will be influenced by the loss of the antennas and (21) is no longer valid. However, in the FD, as we can see from (4), (6) and (7), the antenna efficiency has been calibrated out in the net

PTF. Thus, it is not necessary for the antennas to be of high efficiency. Moreover, the proposed methods are general for SE measurement no matter the SE is low or high. The measurement uncertainty is only determined by the dynamic range of the VNA. When the EUT is well shielded, the power coupled from the RC into the EUT will be very small. Consequently, S_{31} will be very small. Under this circumstance, The VNA used in the measurement should have a large dynamic range to measure the small S_{31} accurately. Or, the measured SE could be of big error. Finally, during the measurement, the antennas (especially the one in the EUT) should be placed away from the conducting walls of the cavities (at least quarter-wavelength distance from the nearest walls for the lowest frequency) to avoid the boundary effect [25], [26].

In future work, we will investigate the industrial applications of the proposed simplified methods for real reverberant environments such as the below-deck compartments in ships and aircraft cabins and bays.

REFERENCES

[1] *IEEE Standard Method for Measuring the Effectiveness of Electromagnetic Shielding Enclosures*, IEEE Standard 299, 2006.

[2] D. A. Hill, M. T. Ma, A. R. Ondrejka, B. F. Riddle, M. L. Crawford, and R. T. Johnk, "Aperture excitation of electrically large, lossy cavities," *IEEE Trans. Electromagn. Compat.*, vol. 36, no. 3, pp. 169–178, Aug. 1994.

[3] D. A. Hill, *Electromagnetic Fields in Cavities: Deterministic and Statistical Theories*. New York, NY, USA: IEEE Press, 2009.

[4] C. L. Holloway, D. A. Hill, M. Sandroni, J. M. Ladbury, J. Coder, G. Koepke, A. C. Marvin and Y. He, "Use of Reverberation Chambers to Determine the Shielding Effectiveness of Physically Small, Electrically Large Enclosures and Cavities," *IEEE Trans. Electromagn. Compat.*, vol. 50, no. 4, pp. 770-782, Nov. 2008.

[5] Q. Xu, Y. Huang, X. Zhu, L. Xing, Z. Tian and C. Song, "Shielding Effectiveness Measurement of an Electrically Large Enclosure Using One Antenna," *IEEE Trans. Electromagn. Compat.*, vol. 57, no. 6, pp. 1466-1471, Dec. 2015.

[6] C. L. Holloway, D. A. Hill, J. Ladbury, G. Koepke and R. Garzia, "Shielding effectiveness measurements of materials using nested reverberation chambers," *IEEE Trans. Electromagn. Compat.*, vol. 45, no. 2, pp. 350-356, May 2003.

[7] J. Carlsson, K. Karlsson and A. Johansson, "Validation of shielding effectiveness measurement method using nested reverberation chambers by comparison with aperture theory," in *Proc. IEEE Int. Symp. Electromagn. Compat.*, Sept. 2012, pp. 1-6.

[8] G. B. Tait, R. E. Richardson, M. B. Slocum and M. O. Hatfield, "Time-Dependent Model of RF Energy Propagation in Coupled Reverberant Cavities," *IEEE Trans. Electromagn. Compat.*, vol. 53, no. 3, pp. 846-849, Aug. 2011.

[9] S. Greco and M. S. Sarto, "Hybrid Mode-Stirring Technique for Shielding Effectiveness Measurement of Enclosures Using Reverberation Chambers," in *Proc. IEEE Int. Symp. on Electromagn. Compat.*, Jul. 2007, pp. 1-6.

[10] *Electromagnetic Compatibility (EMC) Part 4-21: Testing and Measurement Techniques-Reverberation Chamber Test Methods*, IEC 61000-4-21, 2003.

[11] Z. Tian, Y. Huang, Y. Shen and Q. Xu, "Efficient and Accurate Measurement of Absorption Cross Section of a Lossy Object in Reverberation Chamber Using Two One-Antenna Methods," *IEEE Trans. Electromagn. Compat.*, vol. 58, no. 3, pp. 686-693, Jun. 2016.

[12] C. L. Holloway, H. A. Shah, R. J. Pirkl, W. F. Young, D. A. Hill and J. Ladbury, "Reverberation Chamber Techniques for Determining the Radiation and Total Efficiency of Antennas," *IEEE Trans. Antennas Propag.*, vol. 60, no. 4, pp. 1758-1770, Apr. 2012.

[13] P. S. Kildal, X. Chen, C. Orlenius, M. Franzen and C. S. L. Patane, "Characterization of Reverberation Chambers for OTA Measurements of Wireless Devices: Physical Formulations of Channel Matrix and New Uncertainty Formula," *IEEE Trans. Antennas Propag.*, vol. 60, no. 8, pp. 3875-3891, Aug. 2012.

[14] Y. Huang and D. J. Edwards, "A novel reverberating chamber: the source-stirred chamber," *8th Int. Conf. Electromagn. Compat.*, Edinburgh, 1992, pp. 120-124.

[15] D. A. Hill, "Electronic mode stirring for reverberation chambers," *IEEE Trans. Electromagn. Compat.*, vol. 36, no. 4, pp. 294-299, Nov. 1994.

[16] C. R. Dunlap, "Reverberation chamber characterization using enhanced backscatter coefficient measurements," Ph.D. dissertation, Dept. of Elect. Comput. and Eng., Univ. of Colorado, Boulder, USA, 2013.

[17] C. R. Dunlap, C. L. Holloway, R. Pirkl, J. Ladbury, E. F. Kuester, D. A. Hill, and S. van de Beek, "Characterizing reverberation chambers by measurements of the enhanced backscatter coefficient," in *Proc. IEEE Int. Symp. on Electromagn. Compat.*, Aug. 2012, pp. 210-215.

[18] G. B. Tait, R. E. Richardson, M. B. Slocum, M. O. Hatfield and M. J. Rodriguez, "Reverberant Microwave Propagation in Coupled Complex Cavities," *IEEE Trans. Electromagn. Compat.*, vol. 53, no. 1, pp. 229-232, Feb. 2011.

[19] J. S. Giuseppe, C. Hager and G. B. Tait, "Wireless RF Energy Propagation in Multiply-Connected Reverberant Spaces," *IEEE Antennas Wireless Propag. Lett.*, vol. 10, pp. 1251-1254, 2011.

[20] R.Richardson, "Reverberant microwave propagation," Naval Surface Warfare Center, Dahlgren Division, Dahlgren, VA, Tech. Rep. NSWCDD/TR-08/127, Oct. 2008.

[21] A. H. Davis, "Reverberation equations for two adjacent rooms connected by an incompletely soundproof partition," *Philos. Mag.*, vol. 50, no. 295, pp. 75–80, Jul. 1925.

[22] A. D. Pierce, *Acoustics: An Introduction to Its Physical Principles and Applications*. New York: McGraw-Hill, 1981, ch. 6.

[23] C. L. Holloway, H. A. Shah, R. J. Pirkl, K. A. Remley, D. A. Hill and J. Ladbury, "Early Time Behavior in Reverberation Chambers and Its Effect on the Relationships Between Coherence Bandwidth, Chamber Decay Time, RMS Delay Spread, and the Chamber Buildup Time," *IEEE Trans. Electromagn. Compat.*, vol. 54, no. 4, pp. 714-725, Aug. 2012.

[24] S. J. Boyes, "Reverberation Chambers and the Measurement of Antenna Characteristics," Ph.D. dissertation, Dept. of Elect. Eng. and Electron., Univ. of Liverpool, Liverpool, U.K., 2013.

[25] D. A. Hill, "Boundary fields in reverberation chambers," *IEEE Trans. Electromagn. Compat.*, vol. 47, no. 2, pp. 281-290, May 2005.

[26] A. Somani, S. Gorla, M. Magdowski and R. Vick, "Measurement of boundary fields in a reverberation chamber," in *Proc. IEEE Int. Symp. on Electromagn. Compat.*, Sept. 2011, pp. 123-127.